LASER & PHOTONICS REVIEWS

www.lpr-journal.org

Absolute Time Delay Measurement Over an Existing Radio Over Free-Space Optical Link with Sub-Picosecond Precision

*Zhongyang Xu, Xiuyuan Sun, Yawei Zhang, Bowen Qiu, Yue Yang, Xiangchuan Wang, and Shilong Pan**

Distributed RF systems are referred to as the fundamental structure for future wireless communication and sensors. To enable wideband coherent operation, synchronization across the distributed systems with massive parallel absolute time delay (ATD) measurements up to sub-picosecond precision should be implemented. Traditional ways to achieve precise ATD measurements usually rely on probe signals with broad bandwidth, while that of RF systems is limited. Although an all-optical solution has high precision, it is complex and not compatible with RF systems. Microwave photonics, which combines the merits of RF and photonics, potentially provides a low-cost and high-precision solution that can be deployed in existing RF systems. Here, ATD measurement with sub-picosecond precision directly over an existing radio over free-space optical (RoFSO) link, requiring no additional hardware beyond the link, is achieved. The bandwidth of the system is only 10 MHz, while the measurement results meet well with those obtained by optical combs. The measurement errors caused by atmospheric turbulence are well suppressed by a dynamic Kalman filter. The RoFSO links can be stabilized in a closed-loop measurement. The standard deviation of the timing jitter is 0.28 ps, and the Allan variance is around 1.9×10^{-19} @ 1000 s, which is sufficient to synchronize millimeter-wave signals.

1. Introduction

Distributed systems that consist of separate nodes provide exceptionally enhanced power efficiency, flexibility, reliability, resolution, and coverage, enabling applications such as mobile navigation, multistatic radar,[1] B5G wireless communication systems,[2] and very long baseline interferometry.[3,4] Time synchronization and node positioning enable a coherent distributed system, which provides significant gain in signal-to-noise ratio (SNR) over a monostatic system. Especially, when N identical nodes are coherently combined in a distributed network, an N^3 SNR improvement can be acquired in theory, which enhances substantially the sensitivity of distributed phased radars.[5,6] However, the performance of the coherent distributed system severely degrades when the synchronization and positioning errors are larger than 1/10 of the wavelength. Hence, absolute time delay (ATD) measurement is required to realize such high-precision time synchronization and positioning. Previously, ATD measurement with sub-nanosecond precision was achieved through RF links,[7] satellite-based solutions,[8] or algorithm-based solutions.[9] With the increase of the carrier frequency, the sub-nanosecond precision is inadequate to ensure the coherence operation at the millimeter-wave band, which requires ATD measurement with sub-picosecond precision. Unfortunately, traditional ways to achieve precise ATD measurements always rely on probe signals with broad bandwidth,[10,11] while that of RF systems is usually limited.[12]

Recently, photonics is employed in distributed RF systems, showing distinct advantages in terms of large bandwidth, low phase noise, and low-loss propagation as compared to its electronic counterpart, which is beneficial for developing future distributed RF systems.[13,14] Analog optical links, such as radio over fiber (RoF) link and radio over free-space optical (RoFSO) link have been widely used to bridge the separated nodes in the distributed RF systems. Meanwhile, time synchronization and node positioning can also be achieved through the optical link. Previously, the ATDs of optical links have been measured using frequency-chirped optical signals,[15] 1-pulse-per-second (1PPS) optical signals,[16] or optical pseudorandom bit sequences (PRBS).[17,18] The most appealing feature of these solutions is that no additional hardware beyond the existing optical communication or analog optical links is required. However, the precision of the ATD measurement in most of these methods is several picoseconds, which is still inadequate for high-frequency RF systems. Increasing the precision to the sub-picosecond level is almost impossible since the photoelectronic response and the clock jitter of the analog-to-digital converter (ADC) are at the picosecond level.[18] To enhance the precision of the ATD measurement, ultrashort light pulses or optical frequency combs can be employed due to the THz bandwidth.[19–21] ATD can be estimated with femtosecond-level precision in optical two-way

Z. Xu, X. Sun, Y. Zhang, B. Qiu, Y. Yang, X. Wang, S. Pan
Key Laboratory of Radar Imaging and Microwave Photonics, Ministry of Education
Nanjing University of Aeronautics and Astronautics
Nanjing 210016, China
E-mail: pans@nuaa.edu.cn

The ORCID identification number(s) for the author(s) of this article can be found under https://doi.org/10.1002/lpor.202200835

DOI: 10.1002/lpor.202200835

time-frequency transfer (O-TWTFT).[10,22,23] However, the system demands additional transmitters, receivers, and signal processors.[24] For example, two optical combs are, respectively, used in two sites, and a third comb is used in the local site for optical sampling, which boosts the cost of the system.[25]

For a distributed RF network that has multiple stations and connections, massive parallel ATD measurements should be implemented for collaborative signal processing. Moreover, in applications such as radars in the millimeter-wave band or below, the femtosecond level precision is superfluous.[18] Therefore, compared to the comb-based solutions, a simple and low-cost ATD measurement system with sub-picosecond precision that is compatible with the existing RF systems would greatly promote the popularization of distributed RF systems. In 2019, we demonstrated optical transfer delay measurement directly over an RoF link based on phase-derived ranging,[26] by which the measurement accuracy in a 34 km optical fiber was less than 0.1 ps.[27] The proposed method achieves high-precision measurement with a narrowband signal, while barely changing the hardware, which is attractive to be applied in a distributed RF system.

However, the phase-derived solution is difficult to be used in a RoFSO link, since the atmospheric turbulence not only changes the time delay,[28,29] but also causes optical intensity scintillation, beam wanders, and fluctuations of the angle-of-arrival,[30] leading to severe optical power fluctuations and deep power fading.[31] The deep power fading can be overcome in the comb-based solutions because the time and phase information can be reconstructed from the remaining pulses.[22] Nevertheless, in the phase-derived solution, since continuous light wave is used, the power and phase fluctuations are coupled with each other in RoFSO links so that the precision of the RF phase discrimination is seriously impaired.[32] The impacts of the power fluctuations must be mitigated so that the ATD can be precisely measured using the phase-derived method directly over the RoFSO link.

In this paper, we achieve ATD measurement of RoFSO links with sub-picosecond precision based on phase-derived ranging. A 1 km RoFSO link is consecutively monitored over hours, in which the measured results meet well with that obtained by optical frequency combs. The carrier frequency and bandwidth of the ATD measurement system are 1 GHz and 10 MHz, respectively. Dynamic Kalman filtering is used to mitigate the impacts of intensity fluctuations so that the timing jitter caused by the atmospheric turbulence can be characterized. It is found that the timing jitter follows different turbulence theories when the tip-tilt stabilization is turned on or off, which indicates that the tip-tilt stabilization causes additional low-frequency noise. The high-precision ATD measurement can also be used for time synchronization through the RoFSO links. In a closed-loop measurement, the ATD of the RoFSO link can be stabilized over 14 000 s (more than 3 h) with a standard deviation of 0.11 ps. Moreover, the ATD of the stabilized RoFSO link is tested by another independent system. The ATDs fluctuate with a peak-to-peak wander of 1.3 ps and a standard deviation of 0.28 ps. Allan variances are also calculated based on the measured ATD, which is reduced to 1.9×10^{-19} @ 1000 s by the active stabilization. Compared to the comb-based solutions, the measurement system is simple, sharing many RF components with the existing RoFSO link. Moreover, only common RF devices and MHz-level bandwidth are used, making the system low-cost and convenient to apply massively in distributed RF networks.

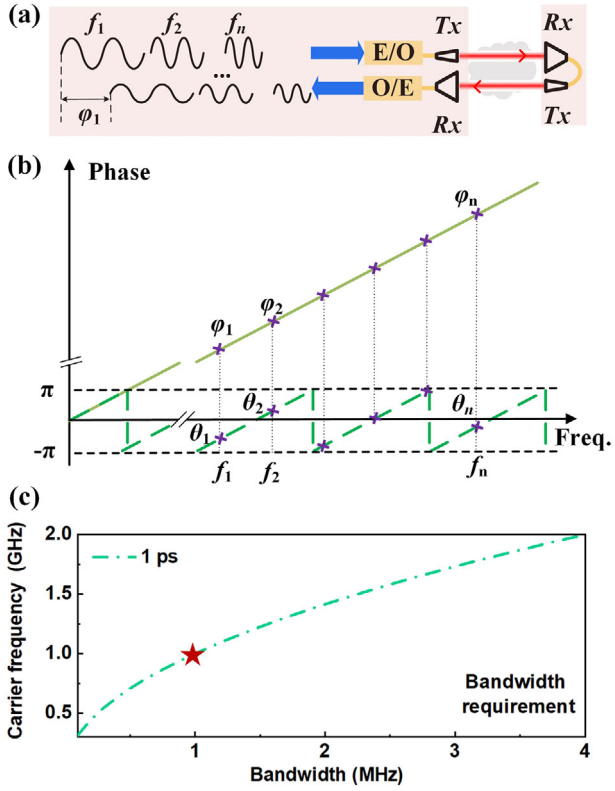

Figure 1. Principle of the ATD measurement over a RoFSO link. a) Schematic diagram of the ATD measurement system. Tx: transmitter, Rx: receiver, E/O: electro-optic modulation, O/E: optoelectronic detection. b) Principle of the phase unwrapping algorithm. c) The bandwidth required to achieve the sub-picosecond precision (solid line). If the carrier frequency is 1 GHz, 1-MHz bandwidth is sufficient (red star).

2. Principle and Experiment

Figure 1 illustrates the principle of the ATD measurement over an existing RoFSO link. The intensity of an optical carrier is firstly modulated by an RF signal. Then, the modulated optical signal propagates round-trip through the RoFSO link. In the receiver, the RF signal is recovered from the intensity of the optical signal. Finally, the ATD of the round-trip optical path is obtained from the absolute phase delay of the recovered RF signal. Since a microwave phase discriminator (MPD) is used, the measurement range of phase is from $-\pi$ to π. The absolute phase delay is then written as

$$\varphi = 2\pi N + \theta \tag{1}$$

where θ is the wrapped phase delay that is measured by the MPD, and N is an unknown integer.

To overcome the 2π phase ambiguity, a frequency-swept RF signal is used in the phase-derived ranging. The wrapped phases θ_i (dashed lines in Figure 1b) are measured at different frequencies f_i. Then, the value of N is calculated using a phase unwrapping algorithm.[27] Finally, the absolute phase delays (unwrapped

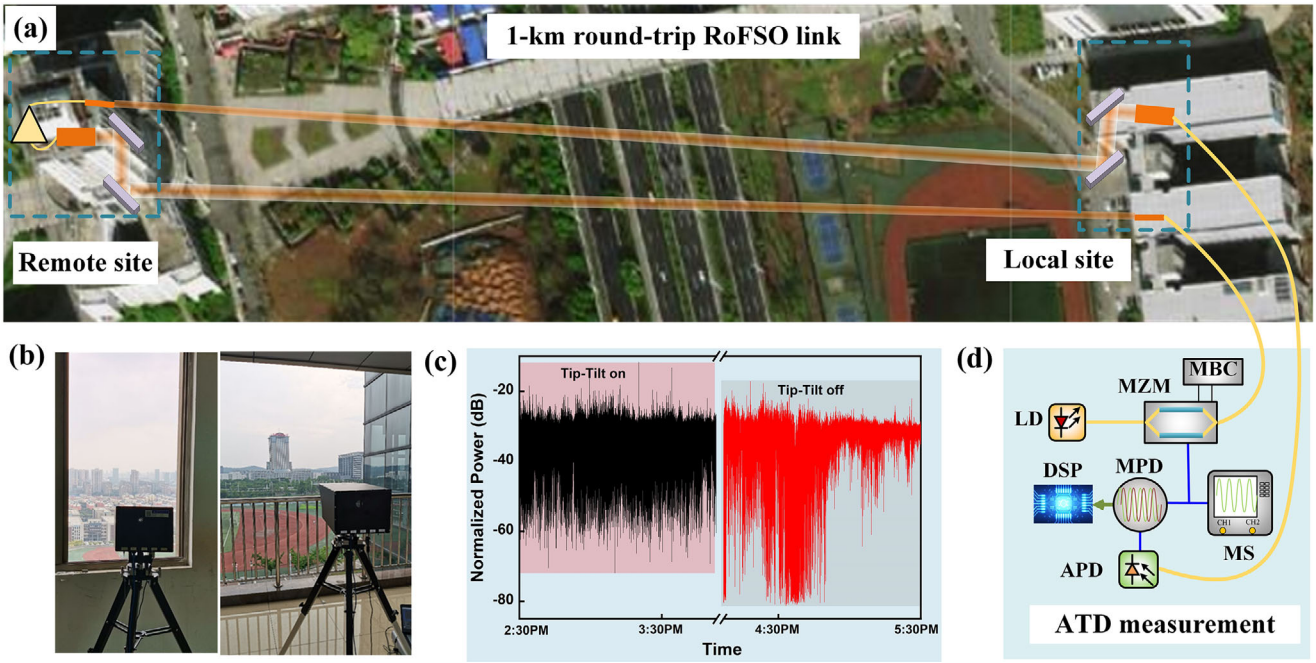

Figure 2. ATD measurement of a 1 km RoFSO link between two buildings. a) Image of the 1 km round-trip air path. b) Photographs of the local site (right) and remote site (left). c) The optical power of the received light in the local site. Tip-tilt stabilization is turned on from 2:30 to 3:40 PM, while it is turned off from 4:20 PM to 5:30 PM. d) Block diagram of the ATD measurement system based on the phase-derived ranging. LD: laser diode, MZM: Mach–Zehnder modulator, MBC: modulator bias controller, APD: avalanche photodiode detector, MS: microwave source, MPD: microwave phase discriminator, DSP: digital signal processor.

phases) φ_i at different frequencies are obtained. The ATD can be calculated as[26]

$$\tau = \left(N_{\mathrm{M}} + \frac{\theta_{\mathrm{M}}}{2\pi}\right)\frac{1}{f_{\mathrm{M}}} \tag{2}$$

where f_{M} is the maximum frequency that is used in the measurement, θ_{M} is the wrapped phase measured at f_{M}, and N_{M} can be calculated at f_{M} by the phase unwrapping algorithm. The measurement precision depends on the precision of the MPD, which is better than ±0.1°. The unambiguous range of the measurement is determined by the frequency interval ($f_i - f_{i-1}$). 1 kHz frequency sweep interval leads to a measurement range of 500 µs (i.e., 150 km). Moreover, to ensure the phase unwrapping, the span range of the frequency-swept RF signal should satisfy[26]

$$f_{\mathrm{span}} > \Delta\tau f_{\mathrm{M}}^2 \tag{3}$$

where f_{span} is the frequency span, and $\Delta\tau$ is the precision of the ATD which depends on the precision of phase discrimination. Figure 1c shows the bandwidth requirement for 1 ps precision (solid line). It should be noted that the required bandwidth is only 1 MHz to achieve sub-picosecond precision if the carrier frequency is 1 GHz (red star in Figure 1c). Therefore, a low-frequency and narrowband signal can be used in the ATD measurement system, which barely occupies the bandwidth of the existing RoFSO link. (The detailed mathematical derivations are described in Note S1, Supporting Information).

A RoFSO link is built between two buildings at the Nanjing University of Aeronautics and Astronautics (NUAA) campus (see detailed descriptions in Note S2, Supporting Information). As shown in **Figure 2**a, the air path passes over grass, trees, and a high-speed way. The length of the round-trip air path is around 1 km. Two optical terminals with a tip-tilt stabilization system are, respectively, used in the local site and remote site, as illustrated in Figure 2b. The elevation of the laser beam varies from 20 to 100 m, and the lateral distance between the forward and backward propagating laser beams is around 20 cm. Figure 2d depicts the block diagram of the ATD measurement system. A 1550 nm continuous-wave light from a narrow-linewidth laser diode (LD) is used as the optical carrier, and a frequency-swept RF signal with a center frequency of 1 GHz is generated by a microwave source (MS), which is used to modulate the optical carrier in a Mach–Zehnder modulator (MZM). An avalanche photodiode detector (APD) is used to recover the frequency-swept RF signal. Finally, the wrapped phase delay is extracted by an MPD, and the ATD is calculated by a digital signal processor (DSP). The precision of the MPD is ±0.1°. The frequency interval and the bandwidth of the frequency-swept RF signal are 1 kHz and 10 MHz, which ensures a sub-picosecond precision for the phase-derived solution. It should be noted that high-accuracy ATD measurement can be achieved if the systematic bias caused by fiber patches, electrical cables, and photodetectors is precalibrated. In that case, a high-accuracy ATD measurement can be achieved. Moreover, tip-tilt stabilization is used to mitigate deep power fading, which has been previously applied in stable optical frequency transfer.[32–34] Figure 2c shows the received optical power at the APD. The tip-tilt stabilization is turned on from 2:30 to 3:40 PM, while it is turned off from 4:20 to 5:30 PM. The deep power fading as low as 60 dB frequently comes up when the tip-tilt stabilization

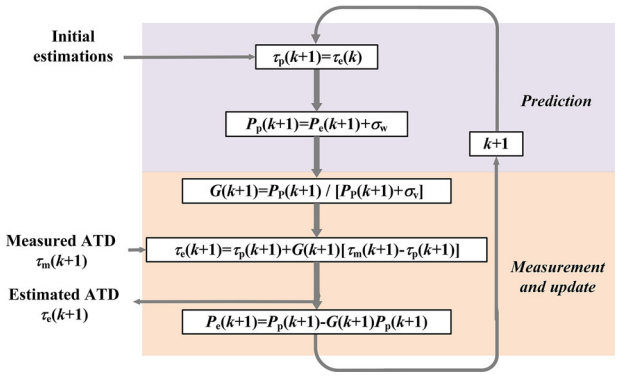

Figure 3. Flow chart of Kalman filtering process. Given the values of σ_w, σ_v, $\tau_e(1)$, and $P_e(1)$, the system output the estimated ATD ($\tau_e(k+1)$).

is turned off. On the other hand, although the optical power still fluctuates in a range of 30 dB, the deep power fading is fully suppressed if the tip-tilt stabilization is turned on.

The 30-dB optical power fluctuations, however, still result in errors in the ATD measurement. Using high-performance tip-tilt stabilization, the power fluctuations can be reduced to 3dB.[32] In the proposed system, we apply Kalman filtering to reduce the measurement errors,[33,35,36] which is an optimal estimation algorithm that extracts useful signals from noisy measurement results.[37,38] To implement the Kalman filtering, a dynamic model is first established based on the statistical characteristics of noise, which consists of a prediction equation and an update equation

$$\tau_p(k+1) = \tau_p(k) + w(k) \tag{4}$$

$$\tau_m(k+1) = \tau_p(k+1) + v(k+1) \tag{5}$$

where k is the number of measurements, τ_p and τ_m are the predicted and measured ATD, respectively. w is the predicted variation of the ATD due to the atmospheric turbulence, and v is the measurement noise induced by the power fluctuations and systematic errors. The flow chart of the Kalman filtering is described in **Figure 3**. In the iterations, τ_e is the estimated ATD, σ_v and σ_w are the covariance of w and v, respectively. It should be noted that the Kalman filtering can run in real time based on the present measurement and the previously calculated state. Hence, the measurement rate is barely reduced (The detailed descriptions for the Kalman filtering are shown in Note S3, Supporting Information).

3. Results and Discussions

3.1. ATD Measurement of the RoFSO Link

High-precision ATD measurement in fiber links based on the phase-derived ranging has previously been demonstrated.[26,27] Here, we use an optical delay line (General Photonics, DL–002 OEM) to test the precision of our system. The ATD can be changed by the optical delay line, of which the resolution is finer than 1 fs and the accuracy is ±0.01 ps. The errors between the measured ATD changes and the actual ATD changes range from

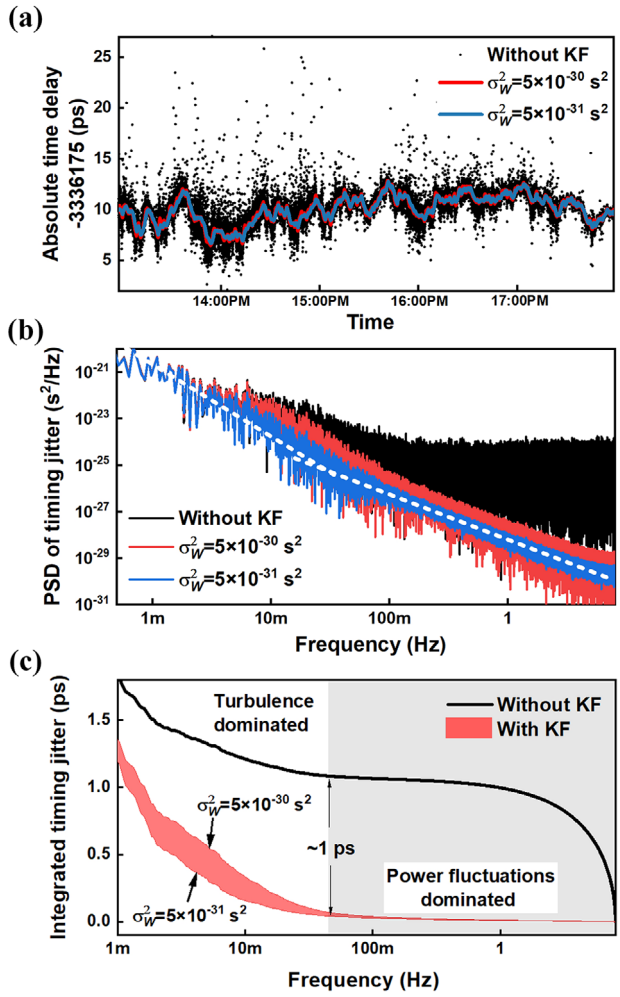

Figure 4. ATD measurement of the RoFSO link. a) The measured ATD without Kalman filter (black scatters). The colored lines are the results after Kalman filtering with different values of σ_w^2. b) The PSD is calculated from the measured ATD. c) The calculated integrated timing jitter. The red shadow indicates the uncertainty of the Kalman filter caused by the uncertainty of C_n^2.

−0.088 to 0.082 ps, which demonstrates that the precision of the phase-derived solution in fiber links is higher than ±0.1 ps. (The detailed descriptions for measurement precision are shown in Note S2, Supporting Information).

However, due to the power fluctuations, significant fluctuations of phase delay can be observed in the APD so that large measurement errors are obtained in the ATD measurement of the RoFSO link. **Figure 4**a shows the measured ATD of the 1 km RoFSO link. The measurement errors of the original results (black scatters) can be as high as 22 ps. The PSD (black line in Figure 4b has a high noise floor at around 10^{-24} s^2 Hz^{-1}, which submerges the timing jitter caused by the atmospheric turbulence. To mitigate measurement errors, a dynamic Kalman filter is adopted. The mean of the first 1000 measurements is used as the value of $\tau_e(1)$, and the value of $P_e(1)$ is set to 1. Since the measurement noise is varied due to the optical power fluctuations, the covariance of the previous 1000 results is used as the value

of σ_v. Therefore, the value of σ_v varies over time. On the other hand, the value of σ_w is calculated based on the turbulence theory as[39,40]

$$\sigma_w^2 = 0.44 C_n^2 D^{5/3} L c^{-2} \quad (6)$$

where C_n^2 is the turbulence structure constant, L is the length of the RoFSO link, and c is the speed of light in vacuum. In the RoFSO link, D is 60 mm, L is 1000 m, and λ is 1550 nm. According to ref. [41] typical values of C_n^2 near the ground range from 10^{-14} $m^{-2/3}$ to 10^{-13} $m^{-2/3}$. As a result, the typical values of σ_w^2 in the Kalman filtering are between 5×10^{-30} s^2 and 5×10^{-31} s^2 (The details about parameter estimation for the Kalman filtering are shown in Note S3, Supporting Information).

In Figure 4a, the results after Kalman filtering are shown as the solid lines, in which the value of σ_w^2 is 5×10^{-30} s^2 and 5×10^{-31} s^2, respectively. The measurement errors are largely reduced. Meanwhile, the noise floors of the PSD are significantly lowered (in Figure 4b). It should be noted that the PSD of the timing jitter caused by the atmospheric turbulence can now be revealed. As the white dashed lines shown in Figure 4b, the PSD after the Kalman filtering follows a −8/3 power law below 50 mHz, which is predicted by Kolmogorov's turbulence theory.[42] Moreover, Figure 4c shows the integrated timing jitter[43] of the PSD from 10 Hz to 1 mHz. Since it is difficult to accurately measure C_n^2,[28] the uncertainty of the Kalman filter mainly arises from the uncertainty of σ_w^2. The red shadow indicates the uncertain range of the integrated timing jitter after Kalman filtering. It should be noted that the integrated timing jitter above 50 mHz is always well reduced which is mainly caused by the power fluctuations, indicating that the impact of the power fluctuations can be well mitigated even though the value of σ_w^2 is not accurately estimated. On the other hand, the integrated timing jitter below 50 mHz that is remained after Kalman filtering is mainly caused by atmospheric turbulence. At 50 mHz, the integrated timing jitter in the power-fluctuations-dominated region is reduced from 1.08 (black line) to 0.06 ps (red lines). Meanwhile, the integrated timing jitter in the turbulence-dominated region is more than 1.02 ps.

To evaluate the measurement precision of the proposed method, the ATD of the 1 km RoFSO link is changed by 1 ps steps every 50 s. The measured results are shown in **Figure 5**a. Without the Kalman filter, the measured ATDs fluctuate in a large range (black scatters) so that the 1 ps step is blurred. But, with the Kalman filter, the fluctuations are significantly suppressed. The variations of the measured ATDs are reduced to less than 1 ps, so the measurement precision is convinced to be higher than 1 ps. Moreover, the measurement result obtained by the comb-based solution is also shown in Figure 5b (red line) for comparison, which is extracted from Figure 4 of ref. [42]. If σ_w^2 is set to 5×10^{-31} s^2 (blue line), the PSD after Kalman filtering is almost overlapped with the result of the comb-based solution in the range from 50 mHz to 10 Hz. In contrast, if σ_w^2 is set to 5×10^{-30} s^2 and 5×10^{-32} s^2, the obtained PSDs (black line and green line) are respectively higher and lower. Because the measurement noise from 50 mHz to 10 Hz is mainly caused by power fluctuations, the dynamic Kalman filter suppresses the effect of power fluctuations very well. The displacement between PSDs in the range

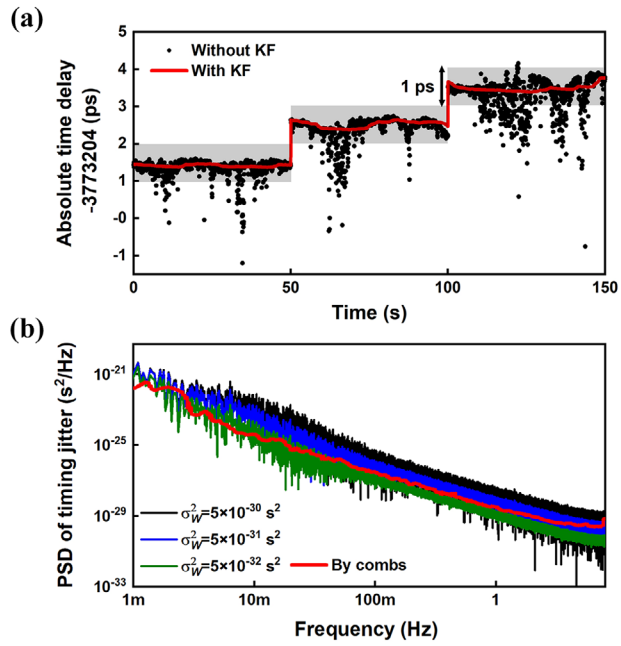

Figure 5. Measurement precision of the proposed method. a) Measured ATDs of the 1 km RoFSO link, which is changed by 1 ps steps. b) PSDs that are measured by the proposed system and comb-based solution. The results obtained by the comb-based solution are extracted from ref. [42].

below 50 mHz is mainly due to the different atmospheric turbulence for different measurements.

3.2. Characterization of the Turbulence-Induced Timing Jitter

Following Taylor's hypothesis of frozen turbulence, the eddies in the atmosphere have a large outer length scale (L_0) and an inner length scale (l_0). The Kolmogorov model is established to describe the atmospheric turbulence between L_0 and l_0, in which the PSD of timing jitter is given by[42]

$$S_{\text{jitter}}(f) = 0.016 C_n^2 L V^{5/3} c^{-2} f^{-8/3}, \quad V/L_0 < f < V/l_0 \quad (7)$$

where L is the length of the air path and V is the wind speed. To extend the Kolmogorov spectrum, von Karman model is given by

$$S_{\text{jitter}}(f) = 0.016 C_n^2 L V^{-1} c^{-2} [(\frac{f}{V})^2 + (\frac{1}{2\pi L_0})^2]^{-4/3}, \quad 0 < f < V/l_0 \quad (8)$$

where the timing jitter in the low-frequency region can be precisely described. (The deduction of the turbulence theory is shown in Note S4, Supporting Information). For RoFSO links, although theories have been established to describe atmospheric turbulence, it is still challenging to characterize the timing jitter in real-time over a wide length scale.[42] The proposed system provides a simple approach for experimental characterization without the use of complex optical frequency combs.

Figure 6 shows the PSDs of timing jitter measured at different times. For comparison, the PSD in the back-to-back measurement is also depicted in Figure 6c, which shows a slope of

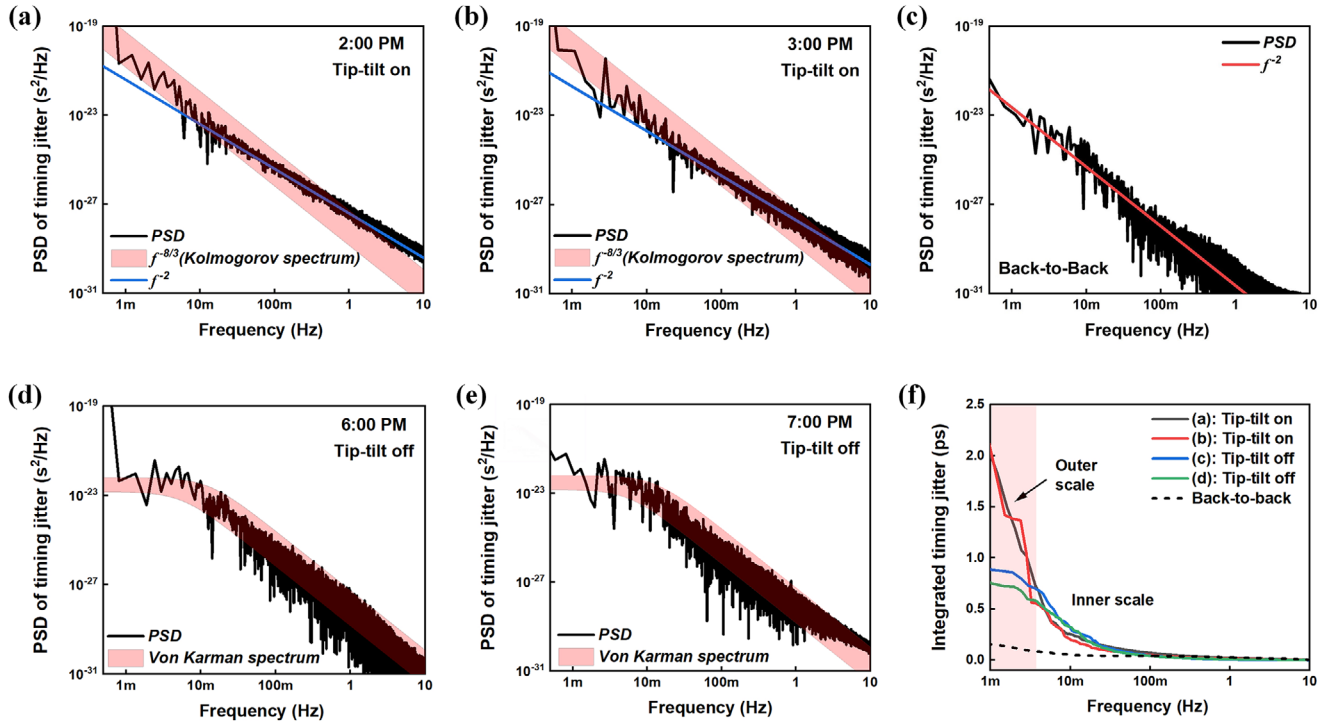

Figure 6. Characterization of the timing jitter. a,b) PSDs of timing jitters measured at 2:00 and 3:00 PM, respectively, when the tip-tilt stabilization is on. c) PSD of the timing jitter for a back-to-back measurement. d,e) PSDs of the timing jitters measured at 6:00 and 7:00 PM, respectively, when the tip-tilt stabilization is off. f) Integrated timing jitter in the range from 10 Hz to 1 mHz for the PSDs in (a, b, d), and e.

−2 that is caused by temperature variations.[32] Figure 6a,b is the measurement results at around 2:00 and 3:00 PM, in which the tip-tilt stabilization is turned on. In the Kalman filter, the value of C_n^2 is set to 4.5×10^{-14} $m^{-2/3}$. Meanwhile, theoretical Kolmogorov spectra are calculated, in which the wind speed is between 3.4 and 7.9 m s^{-1} (according to the weather forecast). C_n^2 is estimated to be between 10^{-14} $m^{-2/3}$ and 10^{-13} $m^{-2/3}$. The red shadows in Figure 6a,b indicate the uncertain range in theoretical Kolmogorov spectra caused by the uncertainty of V and C_n^2. The PSDs after Kalman filtering are almost located in the uncertain ranges and show slopes of −8/3 in the low-frequency range, which agrees well with the Kolmogorov model. Meanwhile, the slopes in the high-frequency range are −2. The turning points depend on the boundaries between the turbulence-dominated and the power-fluctuation-dominated sections, which are 30 and 50 mHz in Figure 6a,b, respectively. The measured turning points are consistent with the results measured by combs.[10,42]

Meanwhile, the ATD is also measured when the tip-tilt stabilization is turned off, which is not been analyzed in previous works.[42] The PSDs are shown in Figure 6d,e. Significantly, the PSDs are flat in the low-frequency range below 10 mHz, which is not consistent with the Kolmogorov spectrum. To fit the PSD, the von Karman spectrum is used. The values of the parameters are the same as that in Figure 6a,b. The red shadows in Figure 6d,e are the uncertain ranges of the theoretical von Karman spectra, which are almost overlapped with the measured results. In addition, Figure 6f shows the corresponding integrated timing jitters from 10 Hz to 1 mHz. When the tip-tilt stabilization is turned off, the integrated timing jitters below 3 mHz (blue and green lines) are lower than 1 ps. In contrast, when the tip-tilt stabilization is turned on, the integrated timing jitters (black and red lines) dramatically rise, which is enlarged from 0.85 to 2.05 ps, indicating that the tip-tilt stabilization causes low-frequency noise and induces a 1.2 ps additional jitter. As a comparison[18,42] the von Karman spectrum is not observed either, in which a tip-tilt stabilization system is always turned on. As the von Karman model predicted, the flat PSD below 10 mHz indicates the impacts of atmospheric turbulence beyond the outer length scale. However, when the tip-tilt stabilization is on, the fluctuations caused by the turbulence beyond the outer length scale are effectively compensated. As a result, the atmospheric turbulence can be regarded as an integral eddy with an infinite outer length scale so that the low-frequency spectrum predicted by the von Karman model no longer exists and extra jitter is caused by the low-frequency noise (see the detailed discussions in Note S5, Supporting Information)

3.3. Applications and Discussions

Based on the high-precision ATD measurement, a closed-loop system can be built, in which active stabilization is implemented to compensate the timing jitter in the RoFSO links (The details about the close-loop system are shown in Note S6, Supporting Information). In **Figure 7**a, without stabilization, the ATD varies in a range of more than 7 ps (black line) during 14 000 seconds in an open-loop system, which randomly spreads with a standard deviation of 1.43 ps (Figure 7b). In contrast, using active stabilization, the fluctuations of the ATDs can be reduced to 0.9 ps (red line)

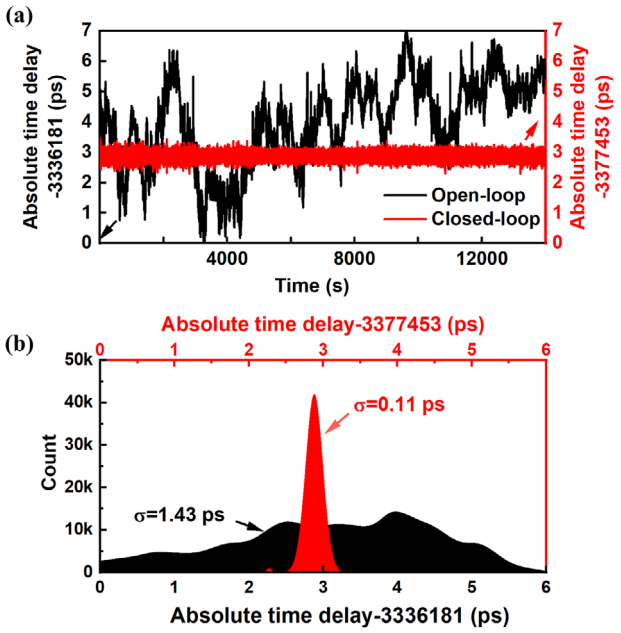

Figure 7. Active stabilization of the 1 km RoFSO link. a) ATDs of the 1 km RoFSO link in the open-loop and closed-loop measurement. b) Distribution histogram of the measured ATDs.

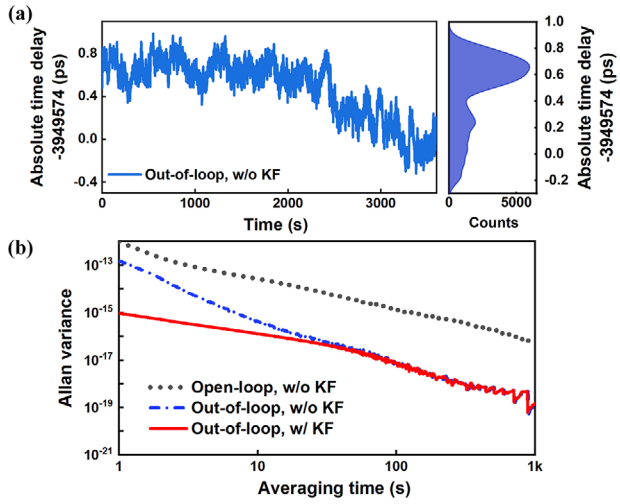

Figure 8. Out-of-loop measurement. a) ATDs of the 1 km RoFSO link measured by a second system. b) Allan variances for the open-loop and out-of-loop measurements. KF: Kalman filter.

Table 1. The performance of ATD measurement methods.

	Comb-based[22]	PRBS[18]	Phase-derived
Precision	1 fs	1 ps	0.1 ps (fiber links)
Stability	4×10^{-19} @1000s [2 km]	1×10^{-15} @1000s [4 km]	1.9×10^{-19} @1000s [1 km]

in a closed-loop system, which follows a normal distribution with a standard deviation of 0.11 ps. Since the variations of the ATDs in the closed-loop system are well compensated, the deviation of the measured ATDs mainly arises from the measurement uncertainty. Therefore, the measurement precision in the closed-loop system is around 0.1 ps, which meets with the result obtained in a fiber link.[26,27]

To test the stability of the stabilized RoFSO link, a second ATD measurement system with a different optical wavelength is established, which is independent of the closed-loop system. (The details about the out-of-loop measurement are shown in Note S6, Supporting Information). The measured ATDs of the stabilized 1-km ROFSO link in an hour are shown in **Figure 8**a, which fluctuate in a range of 1.3 ps, and gradually decreases in the last 1000 s. The standard deviation of the timing jitters is 0.28 ps. This drift is mainly caused by the ATD changes of the fiber patches and electrical cables, which can be reduced by calibration and temperature stabilization. Meanwhile, Allan variances are shown in Figure 8b. In the open-loop system, the Allan variances are around 5.3×10^{-17} @ 1000 s and 1.0×10^{-12} @ 1 s. In the out-of-loop measurement, the Allan variances are 1.9×10^{-19} @ 1000 s and 1.4×10^{-13} @ 1 s, if the Kalman filter is not used. It can be further reduced to 9.1×10^{-16} @ 1 s by the Kalman filter. Hence, the long-term Allan variances of ATD measurement can be reduced by active stabilization, while the short-term Allan variances can be reduced by the Kalman filters.

Table 1 shows the precision and stability of the methods based on optical combs, PRBS, and phase-derived ranging. Undoubtedly, the comb-based method provides the best performance, while the system is the most complex and costly. Using PRBS signals, active synchronization over a 4 km FSO communication channel is achieved with a precision of around 1 ps in ref.[18] The peak-to-peak wander of the ATD is 16 ps over 8 h, and the stability is 1×10^{-15} @ 1000 s. As a comparison, in our system, the peak-to-peak wander of 1.3 ps over 4000 s is achieved. Although the precision is still lower than that of O-TWTFT, the system is simple and low-cost. The major drawback of the proposed system is the low measurement rate, which is only decades of times per second. It can be enhanced to kHz using multifrequency RF phase discrimination.[44]

4. Conclusion

We directly measure the ATD over an existing RoFSO link through atmospheric turbulence. No optical frequency combs are used and the hardware of the RoFSO links is almost not changed. The bandwidth of the ATD measurement system is only 10 MHz and the measurement precision is sub-picosecond. The measurement noise caused by the power fluctuations is well mitigated by a dynamic Kalman filter. Using the high-precision measurement, the timing jitter of a 1 km RoFSO link is characterized, which shows different properties when the tip-tilt stabilization is turned on and off. The measurement results agree well with those obtained by the comb-based solution. In a closed-loop system, the RoFSO link can be well stabilized with a standard deviation of 0.11 ps. Using another independent measurement system, the ATD of the stabilized RoFSO link is measured, showing a peak-to-peak wander of 1.3 ps and a standard deviation of 0.28 ps. The proposed method provides a simple and low-cost approach to measure the ATD of RoFSO

links, which can be applied for time synchronization and node positioning in coherent distributed RF systems.

Supporting Information

Supporting Information is available from the Wiley Online Library or from the author.

Acknowledgements

Z.X. and X.S. contributed equally to this work. This work was financially supported by the National Natural Science Foundation of China (Nos. 62171219, 62075095, 62071226, and 62271249).

Conflict of Interest

The authors declare no conflict of interest.

Data Availability Statement

The data that support the findings of this study are available from the corresponding author upon reasonable request.

Keywords

absolute time delay, distributed RF systems, RoFSO, timing jitter

Received: November 3, 2022
Published online:

[1] J. A. Nanzer, S. R. Mghabghab, S. M. Ellison, A. Schlegel, *IEEE Tran. Microw. Theory Tech.* **2021**, *69*, 4893.
[2] D. R. Brown III, H. V. Poor, *IEEE Trans. Signal Process.* **2008**, *56*, 5630.
[3] H. Hirabayashi, H. Hirosawa, H. Kobayashi, Y. Murata, P. G. Edwards, E. B. Fomalont, K. Fujisawa, T. Ichikawa, T. Kii, J. E. J. Lovell, G. A. Moellenbrock, R. Okayasu, M. Inoue, N. Kawaguchi, S. Kameno, K. M. Shibata, Y. Asaki, T. Bushimata, S. Enome, S. Horiuchi, T. Miyaji, T. Umemoto, V. Migenes, K. Wajima, J. Nakajima, M. Morimoto, J. Ellis, D. L. Meier, D. W. Murphy, R. A. Preston, *Science* **1998**, *281*, 1825.
[4] O. J. Sovers, J. L. Fanselow, C. S. Jacobs, *Rev. Mod. Phys.* **1998**, *70*, 1393.
[5] C. Shi, Y. Wang, S. Salous, J. Zhou, *IEEE Trans. Aerosp. Electron. Syst.* **2022**, *58*, 2762.
[6] R. C. Heimiller, J. E. Belyea, P. G. Tomlinson, *IEEE Trans. Aerosp. Electron. Syst.* **1983**, *19*, 831.
[7] S. M. Ellison, J. A. Nanzer, *IEEE Trans. Aerosp. Electron. Syst.* **2020**, *56*, 4056.
[8] M. Fujieda, T. Gotoh, F. Nakagawa, R. Tabuchi, M. Aida, J. Amagai, *IEEE Tran. Ultrason. Ferroelectr. Freq. Control* **2012**, *59*, 2625.
[9] Y. Yang, R. S. Blum, *IEEE Trans Signal Proces.* **2011**, *59*, 5538.
[10] H. Bergeron, L. C. Sinclair, W. C. Swann, C. W. Nelson, J.-D. Deschênes, E. Baumann, F. R. Giorgetta, I. Coddington, N. R. Newbury, *Optica* **2016**, *3*, 441.
[11] J. Kim, J. A. Cox, J. Chen, F. X. Kartner, *Nat. Photon.* **2008**, *2*, 733.
[12] S. Pan, Y. Zhang, *J. Lightwave Technol.* **2020**, *38*, 5450.
[13] H. Wang, S. Li, X. Xue, X. Xiao, X. Zheng, *Opt. Express* **2020**, *28*, 31241.
[14] X. Xiao, S. Li, S. Peng, D. Wu, X. Xue, X. Zheng, B. Zhou, *Opt. Express* **2018**, *26*, 33783.
[15] S. M. F. Raupach, G. Grosche, *IEEE Trans. Ultrason. Ferroelectr. Freq. Control* **2014**, *61*, 920.
[16] F. Frank, F. Stefani, P. Tuckey, P. Pottie, *IEEE Tran. Ultrason. Ferroelectr. Freq. Control* **2018**, *65*, 1001.
[17] N. Sotiropoulos, C. M. Okonkwo, R. Nuijts, H. de Waardt, J. C. J. Koelemeij, *Opt. Express* **2013**, *21*, 32643.
[18] L. Khader, H. Bergeron, L. C. Sinclair, W. C. Swann, N. R. Newbury, J.-D. Deschênes, *Optica* **2018**, *5*, 1542.
[19] W. Kim, J. Jang, S. Han, S. Kim, J. S. Oh, B. S. Kim, Y.-J. Kim, S.-W. Kim, *J. Opt. Soc. Am. A.* **2020**, *37*, B27.
[20] J. Lee, Y. J. Kim, K. Lee, S. Lee, S.-W. Kim, *Nat. Photonics.* **2010**, *4*, 716.
[21] J. Wang, Z. Lu, W. Wang, F. Zhang, J. Chen, Y. Wang, J. Zheng, S. T. Chu, W. Zhao, B. E. Little, X. Qu, W. Zhang, *Photon. Res.* **2020**, *8*, 1964.
[22] F. R. Giorgetta, W. C. Swann, L. C. Sinclair, E. Baumann, I. Coddington, N. R. Newbury, *Nat. Photon.* **2013**, *7*, 434.
[23] Q. Shen, J. Y. Guan, T. Zeng, Q. M. Lu, L. Huang, Y. Cao, J. P. Chen, T. Q. Tao, J. C. Wu, L. Hou, S. K. Liao, J. G. Ren, J. Yin, J. J. Jia, H. F. Jiang, C. Z. Peng, Q. Zhang, J. W. Pan, *Optica* **2021**, *8*, 471.
[24] A. Abuduweili, X. Chen, Z. Chen, F. Meng, T. Wu, H. Guo, Z. Zhang, *Opt. Express* **2020**, *28*, 39400.
[25] H. Bergeron, L. C. Sinclair, W. C. Swann, I. Khader, K. C. Cossel, M. Cermak, J.-D. Deschênes, N. R. Newbury, *Nat. Commun.* **2019**, *10*, 1819.
[26] S. Li, X. Wang, T. Qing, S. Liu, J. Fu, M. Xue, S. Pan, *IEEE Photon. Technol. Lett.* **2019**, *31*, 1351.
[27] S. Li, T. Qing, J. Fu, X. Wang, S. Pan, *IEEE Trans. Instrum. Meas.* **2021**, *70*, 8000204.
[28] E. D. Caldwell, W. C. Swann, J. L. Ellis, M. I. Bodine, C. Mak, N. Kuczun, N. R. Newbury, L. C. Sinclair, A. Muschinski, G. B. Rieker, *Opt. Express* **2020**, *28*, 26661.
[29] L. Kral, I. Prochazka, K. Hamal, *Opt. Lett.* **2005**, *30*, 1767.
[30] S. Fu, C. Gao, *Photon. Res.* **2016**, *4*, B1.
[31] X. Zhu, J. M. Kahn, *IEEE Trans Commun.* **2002**, *50*, 1293.
[32] B. P. Dix-Matthews, S. W. Schediwy, D. R. Gozzard, E. Savalle, F.-X. Esnault, T. Lévèque, C. Gravestock, D. D'Mello, S. Karpathakis, M. Tobar, P. Wolf, *Nat. Commun.* **2021**, *12*, 515.
[33] L. C. Sinclair, W. C. Swann, H. Bergeron, E. Baumann, M. Cermak, I. Coddington, J. D. Deschênes, F. R. Giorgetta, J. C. Juarez, I. Khader, K. G. Petrillo, K. T. Souza, M. L. Dennis, N. R. Newbury, *Appl. Phys. Lett.* **2016**, *109*, 151104.
[34] H. J. Kang, J. Yang, B. J. Chun, H. Jang, B. S. Kim, Y. J. Kim, S. W. Kim, *Nat. Commun.* **2019**, *10*, 4438.
[35] L. Tao, Z. Liu, W. Zhang, Y. Zhou, *Opt. Lett.* **2014**, *39*, 6997.
[36] L. C. Sinclair, H. Bergeron, W. C. Swann, E. Baumann, J. D. Deschenes, N. R. Newbury, *Phys. Rev. Lett.* **2018**, *120*, 050801.
[37] D. Zibar, J. E. Pedersen, P. Varming, G. Brajato, F. Da Ros, *Optica* **2021**, *8*, 1262.
[38] D. Zibar, H. Chin, Y. Tong, N. Jain, J. Guo, L. Chang, T. Gehring, J. E. Bowers, U. L. Andersen, *IEEE Photon. Technol. Lett.* **2019**, *31*, 1866.
[39] R. J. Noll, *J. Opt. Soc. Am.* **1976**, *66*, 207.
[40] D. L. Fried, *J. Opt. Soc. Am.* **1965**, *55*, 1427.
[41] L. F. Otoniel Canuet, *Ph.D. Thesis*, Universitat Politècnica de Catalunya **2014**.
[42] L. C. Sinclair, F. R. Giorgetta, W. C. Swann, E. Baumann, I. Coddington, N. R. Newbury, *Phys. Rev. A* **2014**, *89*, 023805.
[43] T. K. Kim, Y. Song, K. Jung, C. Kim, H. Kim, C. H. Nam, J. Kim, *Opt. Lett.* **2011**, *36*, 4443.
[44] X. Liu, L. Wang, X. Tang, S. Li, C. Ma, Y. Yang, X. Jiang, C. Huang, X. Wang, S. Pan, presented at ICOCN, Qufu, CHN, August **2021**.